Two-dimensional cross-spectrum of the streamwise velocity in turbulent boundary layers

Rahul Deshpande[1,†], **Dileep Chandran**[1], **Jason P. Monty**[1] **and Ivan Marusic**[1]

[1]Department of Mechanical Engineering, University of Melbourne, Parkville, VIC 3010, Australia

(Received 22 October 2019; revised 15 January 2020; accepted 17 February 2020)

In this paper, we present the two-dimensional (2-D) energy cross-spectrum of the streamwise velocity (u) component and use it to test the notion of self-similarity in turbulent boundary layers. The primary focus is on the cross-spectrum (Φ^{w}_{cross}) measured across the logarithmic (z_o) and near-wall (z_r) wall-normal locations, providing the energy distribution across the range of streamwise (λ_x) and spanwise (λ_y) wavelengths (or length scales) that are coherent across the wall-normal distance. Φ^{w}_{cross} may thus be interpreted as a wall-filtered subset of the full 2-D u-spectrum (Φ), the latter providing information on all coexisting eddies at z_o. To this end, datasets comprising synchronized two-point u-signals at z_o and z_r, across the friction Reynolds number range $Re_\tau \sim O(10^3)$–$O(10^4)$, are analysed. The published direct numerical simulation (DNS) dataset of Sillero *et al.* (*Phys. Fluids*, vol. 26 (10), 2014, 105109) is considered for low-Re_τ analysis, while the high-Re_τ dataset is obtained by conducting synchronous multipoint hot-wire measurements. High-Re_τ cross-spectra reveal that the wall-attached large scales follow a $\lambda_y/z_o \sim \lambda_x/z_o$ relationship more closely than seen for Φ, where this self-similar trend is obscured by coexisting scales. The present analysis reaffirms that a self-similar structure, conforming to Townsend's attached eddy hypothesis, is ingrained in the flow.

Key words: boundary layer structure, turbulent boundary layers

1. Introduction and motivation

Modelling turbulent boundary layers (TBL) has been an increasingly active area of research, leading to proposals of various reduced-order as well as conceptual models. Amongst the latter, the attached eddy model that has evolved from the attached eddy hypothesis (AEH) of Townsend (1976) is well known and provides a kinematic description of the logarithmic (log) region of wall turbulence. It assumes the TBL

† Email address for correspondence: raadeshpande@gmail.com

as an assemblage of randomly distributed geometrically self-similar attached eddies or structures, with their population density inversely proportional to their size (see Marusic & Monty (2019) for a comprehensive review). Throughout this article, the words 'structures', 'eddies' and 'motions' are used interchangeably and essentially refer to the definition of a coherent eddy given by Robinson (1991). Coherent eddies can be self-similar or non-self-similar (Perry, Henbest & Chong 1986; Perry & Marusic 1995). A self-similar eddy refers to a flow structure whose geometric lengths and velocity field scale with distance from the wall (z) and friction velocity (U_τ), respectively. A non-self-similar eddy, on the other hand, does not exhibit these characteristics.

Based on the attached eddy model, Perry *et al.* (1986) showed using spectral-overlap arguments that self-similarity leads to a k_x^{-1} scaling in the premultiplied one-dimensional (1-D) u-spectra. Here, k_x is the streamwise wavenumber and u, v and w would refer to the streamwise, spanwise and wall-normal velocity fluctuations respectively, associated with the coordinate system x, y and z. However, the true k_x^{-1} scaling for the u-spectra, representative of the contributions from purely self-similar eddies has been obscured in the previously reported experiments and simulations due to various reasons, namely: (i) spectral aliasing (Davidson, Nickels & Krogstad 2006; Chandran *et al.* 2017) and (ii) overlapping contributions from various eddy types at finite Re_τ (Perry *et al.* 1986; Perry & Marusic 1995; Baars & Marusic 2020). The present study tests the notion of self-similarity by bypassing both the aforementioned scenarios through a methodology discussed ahead.

The 1-D spectra represents the average energy contribution over the entire range of k_y, for a particular k_x, making it susceptible to spectral aliasing (Tennekes & Lumley 1972). In that respect, a better alternative to the 1-D u-spectrum is the direct measurement of the 2-D u-spectrum as a function of both k_x $(= 2\pi/\lambda_x)$ and k_y $(= 2\pi/\lambda_y)$. The 2-D spectrum, however, is difficult to measure experimentally at high Re_τ. Chandran *et al.* (2017) were able to measure 2-D u-spectra at $2400 \lesssim Re_\tau \lesssim 26\,000$, in the log-region of a zero pressure gradient (ZPG) TBL, by first reconstructing the 2-D two-point correlation:

$$\left.\begin{aligned} R_{u_o u_r}(\Delta x, \Delta y; z_o, z_r) &= \overline{u(x, y, z_r)u(x+\Delta x, y+\Delta y, z_o)}, \\ \text{with } \widetilde{\mathcal{R}}_{u_o u_r} &= R_{u_o u_r}/(\sqrt{\overline{u^2}(z_o)}\sqrt{\overline{u^2}(z_r)}). \end{aligned}\right\} \tag{1.1}$$

Subsequently, the 2-D spectrum was computed by taking the 2-D Fourier transformation of $R_{u_o u_r}$ as:

$$\phi_{u_o u_r}(k_x, k_y; z_o, z_r) = \iint_{-\infty}^{\infty} R_{u_o u_r}(\Delta x, \Delta y; z_o, z_r)\mathrm{e}^{-j2\pi(k_x\Delta x + k_y\Delta y)}\,\mathrm{d}(\Delta x)\,\mathrm{d}(\Delta y), \tag{1.2}$$

where j is a unit imaginary number and overbar denotes ensemble time average. Throughout this article, the 2-D spectrum refers to the modulus of the premultiplied form of $\phi_{u_o u_r}$ normalized by the friction velocity (i.e. $|k_x^+ k_y^+ \phi_{u_o u_r}/U_\tau^2|$). For convenience, the 2-D spectrum for $z_r = z_o$ will be referred to as Φ, while that for $z_r \neq z_o$ will be referred to as Φ_{cross}. In agreement with del Alamo *et al.* (2004), at $Re_\tau \approx 2400$, Chandran *et al.* (2017) observed the constant-energy region of Φ to be nominally bounded by power laws $\lambda_y/z_o \sim (\lambda_x/z_o)^{1/2}$ in the large-scale range: λ_x/z_o, $\lambda_y/z_o > 10$. Here, the wavelengths λ_x and λ_y were interpreted as the surrogate length and width of the energetic eddies in the TBL. Therefore, the observation of a square-root relationship suggested a failure of self-similarity at low Re_τ since it indicates that the eddies do not grow wider (with z) at the same rate as they grow longer. At $Re_\tau \approx 26\,000$, however, they found that the large scales deviate from the square-root relationship towards a linear behaviour ($\lambda_y/z_o \sim \lambda_x/z_o$), which is representative of the self-similarity. The large-scale range where this change occurs was referred to as the large-eddy region, existing in the nominal range $\lambda_x > 10z_o$ and $\lambda_x < 7\delta$ (Chandran *et al.* 2017; Chandran 2019).

Chandran *et al.* (2017) conjectured that clear evidence of self-similarity would be observed only for a TBL at $Re_\tau \gtrsim 60\,000$, due to $\Phi(z_o)$ comprising energy contributions from various eddy types existing at z_o, which obey different scalings (Baars & Marusic 2020). These contributions overlap with one another at relatively lower Re_τ ($\lesssim 60\,000$), due to the limited scale separation, obscuring any $\lambda_y/z_o \sim \lambda_x/z_o$ relationship that may be present. The issue relates to the second reason ((ii) mentioned above) responsible for obscuring self-similar trends in previous studies, and we attempt to resolve it here by 'filtering' out the energy contribution from the non-self-similar structures to bring out the self-similarity unequivocally. Here, the term 'filter' is used to refer, in general, the methodology adopted to extract flow statistics at z_o contributed by structures coherent across a specified wall-normal range, say z_r–z_o. Different studies have adopted different approaches to 'filter' out these non-self-similar contributions, with some making use of the wall filter. Here, the prefix 'wall' before 'filter' refers to the methodology utilized for extracting flow features (at z_o) contributed by eddies extending all the way down to the wall ($z_r \rightarrow 0$). These are referred to as the wall-attached structures in the present manuscript. Similarly, structures which physically do not extend to the wall will be referred as wall-detached structures.

Two recent studies, utilizing the wall filter, have shown promising results with respect to removing the non-self-similar contributions. The first is by Hwang & Sung (2018), who following the works of del Alamo *et al.* (2004) and Lozano-Durán, Flores & Jiménez (2012), implemented a wall filter in their instantaneous ZPG TBL DNS fields at $Re_\tau \approx 1000$ to extract only those energetic motions which were physically attached to the wall. Analysis of these filtered fields revealed a linear relationship between the streamwise and spanwise length scales for the large wall-attached structures. This evidence led them to conclude that the extracted structures were principal candidates for Townsend's AEH. The structures from the $Re_\tau \approx 1000$ DNS, however, are likely not statistically dominant in the log-region due to an insufficient scale separation (Hwang & Sung 2018), encouraging a similar analysis at higher Re_τ. The second study, by Baars, Hutchins & Marusic (2017), involved computing the 1-D linear coherence spectrum from synchronized two-point u-signals acquired at a near-wall and log-region reference location. They identified the characteristic lengths of the energetic wall-attached structures to be scaling self-similarly with z_o, as $\lambda_x/z_o \approx 14$. The analysis, which spanned datasets across three decades of Re_τ, led to the conclusion that a 'self-similar attached eddy structure is ingrained within the TBL flow'. Agostini & Leschziner (2017) made similar observations for structures in the mesolayer. The present study may be viewed as a first step towards the extension of the work by Baars *et al.* (2017) to the 2-D scenario. Here, we study the 2-D cross-spectrum, Φ^w_{cross} (i.e. $z_r \neq z_o$; superscript 'w' used when $z_r^+ \lesssim 15$) by considering z_r in the near-wall region and z_o in the log-region. Therefore, $\Phi^w_{cross}(z_o, z_r)$ shows the 2-D distribution of energy contributed purely by the wall-attached eddies that extend up to z_o and beyond (with $z_o \gg z_r$), and is investigated here to test the notion of self-similarity. Throughout the article, superscript '+' indicates normalization by viscous length (ν/U_τ) and velocity (U_τ) scales.

ZPG TBL dataset acquired at HRNBLWT, $Re_\tau \approx 15\,000$ ($\mathcal{E}_1$):

Set-up	z_o^+	z_r^+	U_∞ (m s^{-1})	δ (m)	TU_∞/δ	l^+	$(\Delta y_1)_{min}$	$(\Delta y_4)_{max}$
Φ	**318**	**318**	20	0.36	19 500	22	0.01δ	2.7δ
Φ	$\underline{477}$	$\underline{477}$	20	0.36	19 500	22	0.01δ	2.7δ
Φ	750	750	20	0.36	19 500	22	0.01δ	2.7δ
Φ	1025	1025	20	0.36	19 500	22	0.01δ	2.7δ
Φ	2250*	2250*	20	0.36	19 500	22	0.01δ	2.7δ
Φ^w_{cross}	**318**	15	20	0.36	19 500	22	0	2.5δ
Φ^w_{cross}	$\underline{477}$	15	20	0.36	19 500	22	0	2.5δ
Φ^w_{cross}	750	15	20	0.36	19 500	22	0	2.5δ
Φ^w_{cross}	1025	15	20	0.36	19 500	22	0	2.5δ
Φ^w_{cross}	2250*	15	20	0.36	19 500	22	0	2.5δ

ZPG TBL DNS (Sillero, Jiménez & Moser 2014), $Re_\tau \approx 2000$ ($\mathcal{S}_1$):

	z_o^+	z_r^+	x_{start}	x_{end}	$(\Delta x)_{max}$	$(\Delta x^+)_{min}$	$(\Delta y^+)_{min}$	$(\Delta y)_{max}$
Φ	**120**	**120**	28.4δ	40.3δ	11.9δ	6.5	3.7	7.6δ
Φ_{cross}	**120**	15–77	28.4δ	40.3δ	11.9δ	6.5	3.7	7.6δ

TABLE 1. A summary of the various datasets containing synchronized multipoint u-signals at z_r and z_o for various spanwise offsets, Δy. Terminology has been described in § 2. Values highlighted in bold indicate the approximate z^+-location for the beginning of the log-region, $2.6\sqrt{Re_\tau}$ (Klewicki, Fife & Wei 2009), underlined represent $z^+ \approx 3.9\sqrt{Re_\tau}$ and the ones with superscript (*) represent the upper limit of the log-region, $z^+ \approx 0.15\delta^+$ (Marusic *et al.* 2013).

2. Experimental and numerical data

Two TBL datasets across a decade of Re_τ are considered for analysis in the present study (table 1). The high-Re_τ dataset ($\mathcal{E}_1$) includes 2-D u-spectra (Φ) and first measurements of 2-D u-cross-spectra (Φ^w_{cross}) at $Re_\tau \approx 15\,000$. This dataset was obtained via synchronized multipoint hot-wire measurements in the large Melbourne wind tunnel (HRNBLWT) and the details of these experiments are provided in table 1. Here, l, U_∞ and T denote the hot-wire sensor length, free-stream velocity and total sampling duration, respectively. Boundary layer thickness, δ, and the friction velocity, U_τ, are estimated via the composite fit proposed by Chauhan, Monkewitz & Nagib (2009). 2.5 μm diameter Wollaston hot-wire probes were used for all measurements, which were operated using an in-house Melbourne University Constant Temperature Anemometer at a rate of $\Delta T^+ \equiv U_\tau^2/(\nu f_s) \approx 0.5$, where f_s refers to sampling frequency.

First, two-point measurements with $z_r^+ \approx z_o^+$ were conducted with the aim to obtain Φ at five wall-normal locations in the log-region, by employing the same experimental set-up and methodology used by Chandran *et al.* (2017). Figure 1(*a*i) shows the schematic of the experimental set-up used to reconstruct the corresponding $R_{u_o u_r}$, with four hot-wire probes (*HW*1–4) located at z_o. Following the calibration procedure adopted by Chandran *et al.* (2017), *HW*1, *HW*2 and *HW*4 were calibrated at z_o by using the free-stream calibrated *HW*3 as reference. During experiments, *HW*3 and *HW*4 remained stationary at a fixed spanwise location while *HW*1 and *HW*2 were traversed together in the spanwise direction with logarithmic spacing. u-velocity time series acquired from a pair of hot wires are cross-correlated to obtain the correlation coefficient ($\widetilde{\mathcal{R}}_{u_o u_r}$) as a function of the spanwise spacing Δy (figure 1*b*). At the start of the measurement, *HW*2 and *HW*3 were kept as close as practicably

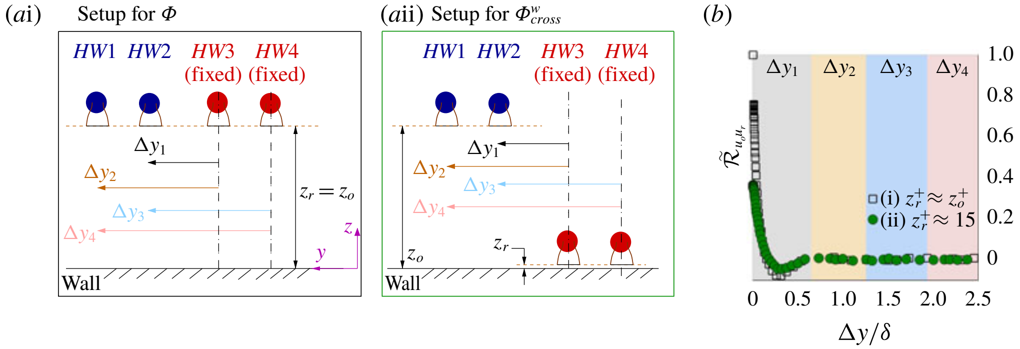

FIGURE 1. (*a*) Schematic of the experimental set-up in HRNBLWT showing relative positioning and movement of the four hot-wire probes (*HW*1–*HW*4) for reconstructing the 2-D correlation corresponding to (i) Φ and (ii) Φ^w_{cross}. Mean flow direction is along x. (*b*) Correlation coefficients ($\widetilde{\mathcal{R}}_{u_o u_r}$) as a function of spanwise separation $\Delta y/\delta$, computed for $z_o^+ \approx 2.6\sqrt{Re_\tau}$ and $\Delta x = 0$.

possible, at $(\Delta y_1)_{min} \approx 0.01\delta$. Thereafter, every step movement of the traverse gives $\widetilde{\mathcal{R}}_{u_o u_r}$ at four distinct spanwise spacings: Δy_1 (*HW*2–*HW*3), Δy_2 (*HW*1–*HW*3), Δy_3 (*HW*2–*HW*4) and Δy_4 (*HW*1–*HW*4). Figure 1(*b*) highlights the Δy range covered by each of these hot-wire pairs with different background colours. The experiment continues up to $(\Delta y_4)_{max} \approx 2.7\delta$, enabling computation of $\widetilde{\mathcal{R}}_{u_o u_r}$ for $\Delta y = 0$ and $(\Delta y_1)_{min} \leqslant \Delta y \leqslant (\Delta y_4)_{max}$. Taylor's hypothesis, with the mean streamwise velocity at z_o considered as the convection velocity, is employed to construct $\widetilde{\mathcal{R}}_{u_o u_r}$ at different streamwise spacings (Δx) for the temporal dataset, $\mathcal{E}_1$. $\Phi(z_o)$ is finally obtained from $R_{u_o u_r}$ via (1.2). It should be noted that $(\Delta y_1)_{min}$ is limited to 0.01δ for the set-up in figure 1(*a*i), which leads to energy redistribution in Φ at small spanwise scales (Chandran *et al.* 2017). To account for this, the DNS-based correction scheme proposed by Chandran *et al.* (2016) has been implemented to correct Φ using the 2-D $\widetilde{\mathcal{R}}_{u_o u_r}$ obtained from the dataset of Sillero *et al.* (2014).

To obtain $R_{u_o u_r}$ corresponding to Φ^w_{cross}, *HW*3 and *HW*4 were fixed at $z_r^+ \approx 15$ while *HW*1 and *HW*2 were positioned at the same z_o^+ (figure 1*a*ii) as in the measurements for Φ. Since the wall-coherence analysis remains largely unaffected for $0 \leqslant z_r^+ \lesssim 15$ (Baars *et al.* 2017), the positioning of the wall-reference probe at $z_r^+ \approx 15$ was considered appropriate. Except for the difference in the wall-normal locations of *HW*3 and *HW*4, the measurement technique to compute $R_{u_o u_r}$ is similar to the previous case. However, for this set-up, $(\Delta y_1)_{min}$ was reduced to zero by vertically aligning *HW*2 above *HW*3. The 1-D linear coherence spectrum (Baars *et al.* 2017) computed from the u-signals acquired by these two probes, at $\Delta y_1 \approx 0$, agreed with its empirical fit proposed by Baars *et al.* (2017), confirming the vertical alignment. Hence, as opposed to Φ, no small-scale correction was required for Φ^w_{cross}. A part of this dataset has also been used recently by Deshpande, Monty & Marusic (2019), wherein the sensitivity of the 1-D linear coherence spectrum to Δy has been showcased.

The low-Re_τ dataset ($\mathcal{S}_1$) considered in the present study is that of Sillero *et al.* (2014). Thirteen raw DNS time blocks are considered, each of which is a subset of the full computational domain between x_{start} and x_{end} (see table 1) to ensure a limited Re_τ increase along x. Table 1 gives more details regarding the spatial resolution and

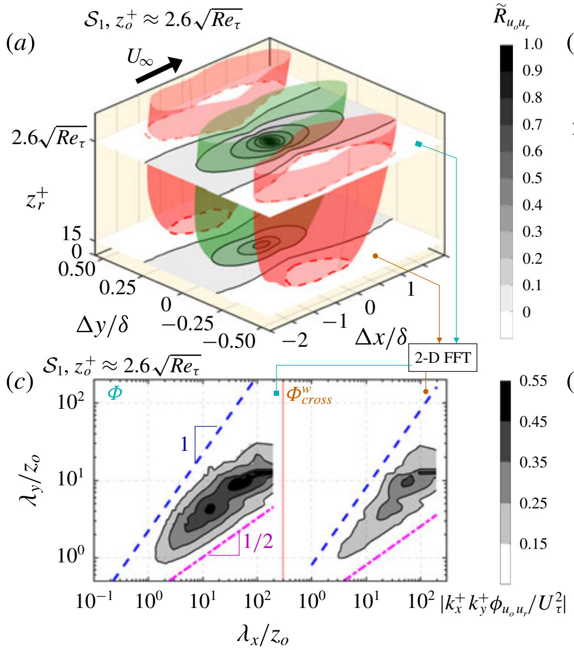

FIGURE 2. (a) 3-D representation of $\widetilde{\mathcal{R}}_{u_o u_r}$ for dataset $\mathcal{S}_1$ with $z_o^+ \approx 2.6\sqrt{Re_\tau}$ ($= 120$) as a reference and $15 \lesssim z_r^+ < 150$ to plot isosurfaces for $\widetilde{\mathcal{R}}_{u_o u_r} = 0.1$ (green) and -0.04 (red). Wall-parallel planes at $z_r^+ \approx 2.6\sqrt{Re_\tau}$ and 15 have positive $\widetilde{\mathcal{R}}_{u_o u_r}$ contours as solid lines at levels 0.0 : 0.1 : 1.0 and a dashed red contour for -0.04. (b) Experimentally ($\mathcal{E}_1$) reconstructed $\widetilde{\mathcal{R}}_{u_o u_r}$ at equivalent z_o^+ and z_r^+ as in (a) and the same contour levels. (c,d) Φ and Φ^w_{cross} for datasets (c) $\mathcal{S}_1$ and (d) $\mathcal{E}_1$ obtained on computing 2-D FFT of the corresponding 2-D $\widetilde{\mathcal{R}}_{u_o u_r}$ plotted in (a) and (b). Contours in (c) and (d) represent energy levels 0.15 : 0.10 : 0.55. Dot-dashed magenta and dashed blue lines represent the square-root and linear relationship, respectively.

size of the flow fields considered. In the case of $\mathcal{S}_1$, Φ and Φ^w_{cross} are computed with $z_o^+ \approx 2.6\sqrt{Re_\tau}$ in order to correspond with $\mathcal{E}_1$. Since we get access to synchronous $u(x, y)$ data at various z in the case of DNS, we also selected several z_r^+ in the range $15 < z_r^+ < z_o^+$ to study the variation in $R_{u_o u_r}$ and the corresponding Φ_{cross}.

3. Results and discussion

3.1. *Physical interpretation of Φ^w_{cross} and how it differs from Φ*

While $\Phi(z_o)$ gives the energy distribution of all coexisting eddies at z_o, Φ^w_{cross} (z_o, z_r) indicates the energy contributed by only those eddies at z_o that have coherence at the wall (i.e. are 'wall-attached'). We attempt to explain this difference by first investigating the cross-correlations, $\widetilde{\mathcal{R}}_{u_o u_r}$. Figure 2($a$) shows the positive and negative isosurfaces of $\widetilde{\mathcal{R}}_{u_o u_r}$ considered from a correlation volume, $\widetilde{\mathcal{R}}_{u_o u_r}(\Delta x, \Delta y, z_r; z_o)$, obtained for $z_o^+ \approx 2.6\sqrt{Re_\tau}$ and $15 \lesssim z_r^+ < 150$ for dataset $\mathcal{S}_1$. The plot is essentially similar in concept to figure 1 of Sillero *et al.* (2014). Considering a wall-parallel plane at $z_r = z_o$ in this correlation volume gives a 2-D $\widetilde{\mathcal{R}}_{u_o u_r}$ map which is analogous to the experimental 2-D correlation obtained via the probe arrangement shown in figure 1(*a*i) and plotted at $z_r^+ \approx 2.6\sqrt{Re_\tau}$ in figure 2(*b*). Now, by considering a wall-parallel plane at $z_r^+ \approx 15$ in figure 2(*a*), we get a 2-D map of *u*-correlation between the log ($z_o^+ \approx 2.6\sqrt{Re_\tau}$) and the near-wall ($z_r^+ \approx 15$) region. An experimental analogue of such a correlation is reconstructed with the probe arrangement shown in figure 1(*a*ii) and is plotted in figure 2(*b*) at $z_r^+ \approx 15$. A qualitative comparison between the respective $\widetilde{\mathcal{R}}_{u_o u_r}$ maps from the two datasets shows good consistency: (i) The length and width of a particular $\widetilde{\mathcal{R}}_{u_o u_r}$ contour level reduces as z_r^+ is varied from z_o^+ towards the wall. This is consistent with the observations of del Alamo *et al.* (2004), who attributed this decrease to the absence of the contributions from wall-detached eddies as $z_r^+ \rightarrow 0$. (ii) The positive *u*-correlations at the spanwise centre ($\Delta y = 0$) are flanked by the negative correlations on either side, which extend all the way from the log-region to the wall. This is representative of the adjacent wall-attached low- and high-momentum zones responsible for the streaky pattern in the TBL (Hutchins & Marusic 2007; Hwang & Sung 2018).

A 2-D Fourier transform of the respective wall-parallel $\widetilde{\mathcal{R}}_{u_o u_r}$ planes in figures 2(*a*,*b*), following (1.2), gives the corresponding 2-D spectral energy distribution plotted in figures 2(*c*,*d*). In each of these plots, $\varPhi$ and $\varPhi^w_{cross}$ as a function of the wavelengths scaled with z_o are plotted on the left and right, respectively. The energy distribution in $\varPhi^w_{cross}$ is restricted to large λ_x and λ_y, with negligible energy in the small scales: $\lambda_x \lesssim 14 z_o$, $\lambda_y \lesssim 2 z_o$, which is unlike the scenario observed for $\varPhi$. This can be explained by $z_o^+ \gg z_r^+$, meaning that only physically large wall-attached eddies would appear in $\varPhi^w_{cross}(z_o)$. In the forthcoming subsection, we compare $\varPhi(z_o)$ and $\varPhi_{cross}(z_o, z_r)$ obtained from the two datasets.

3.2. *Low- versus high-Re_τ 2-D spectra*

Figure 3(*a*) shows the energy spectra for $z_o^+ \approx 2.6\sqrt{Re_\tau}$ and various z_r^+ at a constant energy level of 0.2 for the low-Re_τ dataset ($\mathcal{S}_1$). Also shown are dot-dashed magenta and dashed blue lines which represent the square-root and linear relationship, respectively. As discussed by del Alamo *et al.* (2004) and Chandran *et al.* (2017), constant-energy contours of $\varPhi$ follow a linear relationship ($\lambda_y \sim \lambda_x$) only in the small-scale region: λ_x/z_o, λ_y/z_o < 10. It changes to a square-root relationship ($\lambda_y \sim {\lambda_x}^{1/2}$) at larger scales, suggesting a failure of self-similarity at low Re_τ. On the other hand, if we consider the cross-spectra, the constant-energy contours in the same large-scale range depart from the square-root towards a linear behaviour as z_r approaches the wall (i.e. for $\varPhi^w_{cross}$). This suggests that the energetic wall-attached eddies are predominantly self-similar. Further, this self-similar trend is obscured in $\varPhi$ by energy contributions from the wall-detached eddies. It is obvious, however, that a larger scale separation (i.e. higher Re_τ) would better highlight the changing trend with z_r.

Figure 3(*b*) shows constant-energy contours ($\sim$0.2) of $\varPhi$ and $\varPhi^w_{cross}$ from the high-Re_τ dataset, $\mathcal{E}_1$, with the range of scales increased by almost a decade. Consistent with the observations made by Chandran *et al.* (2017), for the 2-D spectrum $\varPhi$, the square-root relationship for the intermediate range of scales deviates towards a relatively higher power law at $\lambda_x \sim 100 z_o$ and $\lambda_y \sim 15 z_o$, with the large scales having an average aspect ratio of $\lambda_x/\lambda_y \approx 7$ (indicated by a dark yellow line). According to Chandran *et al.* (2017), this ratio is significant since the large-scale energetic structures in a ZPG TBL become self-similar only after evolving into such large aspect ratios. As opposed to $\varPhi$, the energetic ridge of $\varPhi^w_{cross}$ is seen to follow $\lambda_x/\lambda_y = 7$ along its

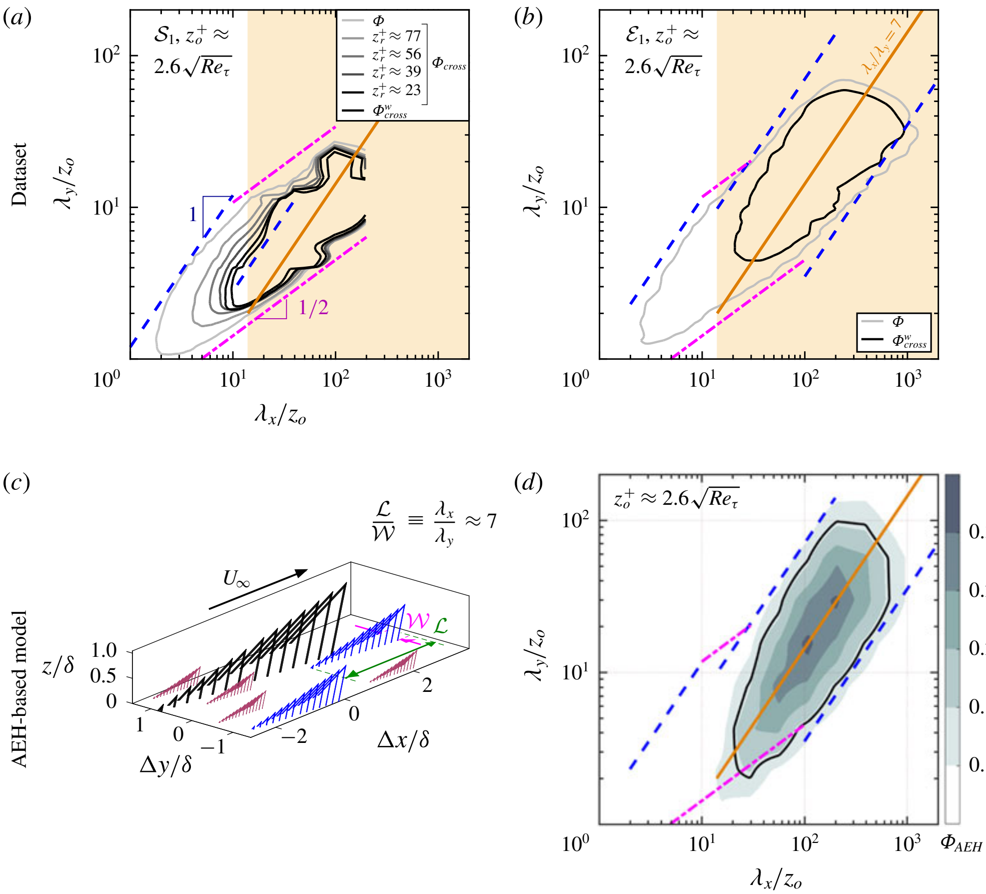

FIGURE 3. (a,b) 2-D energy spectra for $z_o^+ \approx 2.6\sqrt{Re_\tau}$ and various z_r^+ at a constant energy level of 0.2 for datasets (a) $\mathcal{S}_1$ and (b) $\mathcal{E}_1$. Light yellow background indicates $\lambda_x/z_o > 14$. (c) Schematic of the AEH-based model considered, shown here having three distinct hierarchies of self-similar wall-attached eddies, with the largest eddy (in black) of the order of δ. $\mathcal{L}$ and $\mathcal{W}$ denote the length and width of an eddy hierarchy, respectively. (d) 2-D spectra obtained from the AEH-based model for $Re_\tau \approx 15\,000$ and $z_o^+ \approx 2.6\sqrt{Re_\tau}$. Solid black contour is qualitatively equivalent ($\sim 0.5(\Phi_{AEH})_{max}$) to the one in ($b$). In ($a$,$b$,$d$), dot-dashed magenta, dashed blue and solid yellow lines denote $\lambda_y/z_o \sim (\lambda_x/z_o)^{1/2}$, $\lambda_y/z_o \sim \lambda_x/z_o$ and $\lambda_x/\lambda_y = 7$ relationships, respectively.

entire stretch with negligible energy distribution in the scale range where Φ contours vary as $\lambda_y/z_o \sim (\lambda_x/z_o)^{1/2}$. The high-$Re_\tau$ Φ^w_{cross} hence provides convincing evidence of the self-similarity of wall-attached eddies. The fact that the energetic structures contributing to Φ^w_{cross} are restricted to $\lambda_x > 14z_o$ (highlighted by yellow background), which is consistent with the streamwise inner-scaling limit of self-similar wall-attached structures (Baars *et al.* 2017), further adds credence to our claim. Given that Φ^w_{cross} contours follow $\lambda_x/\lambda_y \approx 7$ and $\lambda_x > 14z_o$, present analysis suggests $\lambda_y > 2z_o$ as the plausible spanwise inner-scaling limit for the wall-attached self-similar eddies.

The experimentally obtained Φ^w_{cross} is qualitatively similar to the 2-D energy spectrum (Φ_{AEH}) computed from a flow field consisting purely of self-similar wall-attached eddies, as shown in figure 3(d). Φ_{AEH}, here, is obtained using an AEH-based model

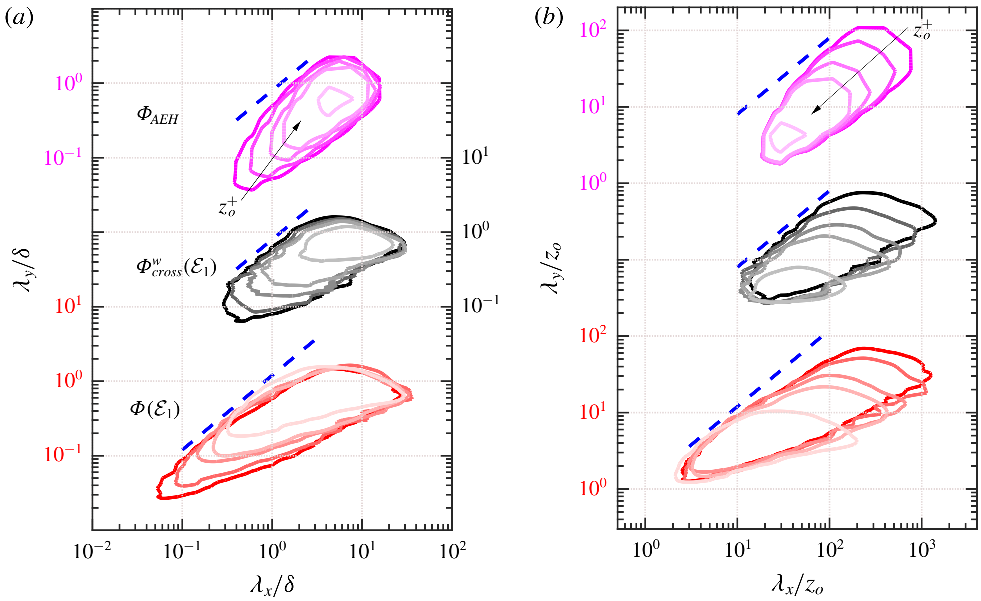

FIGURE 4. (a,b) Contours at a constant energy level of $0.35(\Phi_{AEH})_{max}$, $0.35(\Phi^{w}_{cross})_{max}$ (dataset $\mathcal{E}_1$) and $0.35(\Phi)_{max}$ (dataset $\mathcal{E}_1$) for z_o^+ across the log-region (table 1) plotted as a function of wavelengths scaled with (a) δ and (b) z_o. Dark to light shade indicates an increase in z_o^+. For each of the respective spectra, a maximum value at $z_o^+ \approx 2.6\sqrt{Re_\tau}$ was considered as a reference to normalize the energy spectra at all z_o^+. Dashed blue lines represent the linear power-law relationship for respective spectra.

(Perry *et al.* 1986; Baidya *et al.* 2017; Chandran *et al.* 2017) where the log-region is statistically represented by continuous hierarchies of representative eddies whose geometric sizes scale with z_o and whose probability density varies inversely with z_o. The idea is illustrated in figure 3(c), where, for clarity, the model is depicted in a discretized form with three distinct hierarchies. Heights of the smallest and largest eddies are taken as 100 viscous units and δ, respectively, with each eddy inclined with respect to x at 45° (Deshpande *et al.* 2019). The aspect ratio of the eddy hierarchy is roughly equivalent to the ratio of the large scales observed in the high-Re_τ results. Figure 3(d) plots the 2-D spectrum generated from this model at conditions similar to dataset $\mathcal{E}_1$: $Re_\tau \approx 15\,000$ and $z_o^+ = 2.6\sqrt{Re_\tau}$. It can be noted that the high-Re_τ Φ^{w}_{cross} contours show a good correspondence with Φ_{AEH} contours, which follow the $\lambda_y/z_o \sim \lambda_x/z_o$ relation given the imposition of self-similarity.

We extend this qualitative comparison between Φ^{w}_{cross} and Φ_{AEH} to investigate their scaling in the context of the spectral-overlap arguments of Perry *et al.* (1986). According to their arguments, the energy contribution from self-similar eddies would follow both outer-flow scaling (δ-scaling) and inner-flow scaling (z_o-scaling) in the wavelength range corresponding to $\sim O(\delta)$ and $O(z_o)$, respectively. These scaling arguments are illustrated in figure 4 using Φ^{w}_{cross} and Φ_{AEH}, for all z_o^+ corresponding to $\mathcal{E}_1$ (table 1), wherein the wavelengths are scaled with δ (figure 4a) and z_o (figure 4b) respectively. $\Phi(z_o)$ is also plotted at the same z_o^+ to demonstrate the effectiveness of the wall filter. A noteworthy observation from figure 4 is that both Φ_{AEH} and Φ^{w}_{cross} contours exhibit the δ- and z_o-scalings in a similar wavelength range. This is suggested by the overlapping constant-energy contours for the respective spectra at various z_o^+. Further, these contours indicate an energy distribution predominantly in the large-eddy region (Chandran *et al.* 2017), where they closely follow the $\lambda_y/z_o \sim \lambda_x/z_o$ relationship. This supports the claim that Φ^w_{cross} predominantly consists of the contribution from the self-similar eddies that comply with Townsend's AEH. This contribution can be seen to decrease for both Φ_{AEH} and Φ^w_{cross} as distance from the wall increases, with energy at $z_o^+ \approx 0.15\delta^+$ (light shaded contours) effectively representing the contribution only from the tall wall-attached structures extending beyond the log-region. In the case of Φ, on the other hand, the z_o-scaling is also observed in the small scales, which are predominantly wall-detached and hence do not show up in Φ^w_{cross}. However, the wavelength range exhibiting δ-scaling is similar to that observed for Φ^w_{cross}.

3.3. *Is a wall filter sufficient to extract purely self-similar structures?*

Referring to the discussion in § 1, on the studies by Baars *et al.* (2017) and Hwang & Sung (2018), $\Phi^w_{cross}(z_o)$ may be interpreted as the wall-filtered subset of $\Phi(z_o)$. Recent studies by Baars & Marusic (2020) and Yoon *et al.* (2020) show that not all wall-attached structures exhibit self-similarity, and some of them may be geometrically non-self-similar. Given the qualitative resemblance between Φ^w_{cross} and Φ_{AEH} (§ 3.2), it is worth investigating here if the energy contributions isolated via the wall filter correspond purely to self-similar structures, or there are also contributions from the non-self-similar structures. To this end, we probe the energetic ridges (Chandran *et al.* 2017) of Φ and Φ^w_{cross}, as self-similarity requires the slope (m) of the ridge to be equal to one ($\lambda_y \sim \lambda_x$). Here, the energetic ridge of the spectrum is computed by identifying the spanwise wavelength, λ_y, corresponding to the maximum value of the spectrum at each streamwise wavelength, λ_x. Additionally, Chandran *et al.* (2017) has shown that the slope of the ridge translates as the ratio of the plateaus in the 1-D streamwise u-spectrum to those in the 1-D spanwise u-spectrum. Here, the 1-D streamwise and spanwise spectra are obtained by integrating the 2-D spectrum along λ_y and λ_x, respectively.

Figure 5(*a*) shows the energetic ridges of Φ and Φ^w_{cross} for $z_o^+ \approx 2.6\sqrt{Re_\tau}$, while figure 5(*b*) shows the respective 1-D spectra. A_{1x} and A_{1y} denote the peaks in the 1-D streamwise and spanwise spectra, respectively, while A'_{1x} and A'_{1y} refer to the peaks in the 1-D streamwise and spanwise cross-spectra, respectively. These peaks conform to the scale range where the 1-D spectrum is expected to plateau at very high Re_τ (Chandran *et al.* 2017), and is hence used as a reference over here for analysis purposes. Direct computation of m, from the ratio of the 1-D spectra peaks, shows a difference from 0.7 (for Φ) to 0.85 for Φ^w_{cross}, suggesting a relatively greater contribution from self-similar structures to Φ^w_{cross}. A change in slope is also evident from the comparison between the energetic ridges of Φ and Φ^w_{cross}. Figure 5(*c*) plots m, directly computed from A_{1x}/A_{1y} and A'_{1x}/A'_{1y} for Φ and Φ^w_{cross} respectively, at all z_o^+ corresponding to $\mathcal{E}_1$ (table 1). Here, A_{1x}/A_{1y} can be seen decreasing with an increase in z_o^+. This is consistent with the observations of Chandran *et al.* (2017), who linked this trend with the AEH prediction on the decrease in self-similar eddy population with distance from the wall (Townsend 1976). Interestingly, A'_{1x}/A'_{1y} on the other hand remains approximately constant ($\approx$0.85) at all z_o^+. This suggests that the variation of A_{1x}/A_{1y} with z_o^+ is most likely dictated by the contributions from the wall-detached eddies, which are predominantly small, but can be either self-similar or non-self-similar (Marusic & Monty 2019; Yoon *et al.* 2020).

The increment in m towards 1.0, when comparing Φ and Φ^w_{cross}, confirms that the wall filter does indeed filter out energy contributions from the non-self-similar

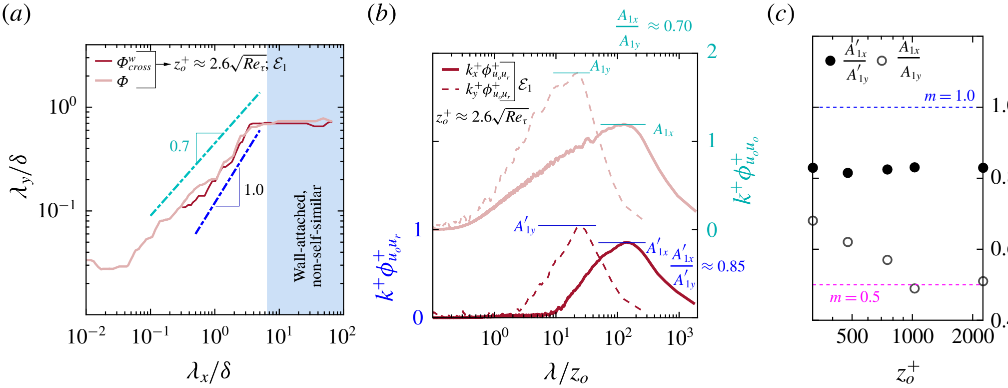

FIGURE 5. (a) Energetic ridges of Φ (light shaded) and Φ^{w}_{cross} (dark shaded) for $z_o^+ \approx 2.6\sqrt{Re_\tau}$ from dataset $\mathcal{E}_1$, plotted against δ-scaled wavelengths alongside the power laws indicated by dot-dashed lines. (b) 1-D spanwise and streamwise (cross-)spectrum obtained on integrating the corresponding Φ (Φ^{w}_{cross}) for $z_o^+ \approx 2.6\sqrt{Re_\tau}$ from $\mathcal{E}_1$. Also highlighted are the peaks of the 1-D spectrum (A_{1x}, A_{1y}) and cross-spectrum (A'_{1x}, A'_{1y}). (c) A_{1x}/A_{1y} and A'_{1x}/A'_{1y} estimated at all z_o^+ corresponding to $\mathcal{E}_1$ (table 1) by following the methodology shown in (b).

structures which are wall-detached. However, the fact that $m \approx 0.85$ and not 1.0 suggests that Φ^{w}_{cross} still consists of contributions from wall-attached non-self-similar structures. This can be better understood on investigating the ridge for Φ and Φ^{w}_{cross} (figure 5a) in the scale range: $\lambda_x \gtrsim 7\delta$, $\lambda_y \sim \delta$, where it appears to plateau at a constant λ_y and grows only in λ_x for both the spectra. The energetic ridge in this scale range is representative of the energy contribution from the δ-scaled superstructures (Hutchins & Marusic 2007; Chandran 2019), which are known to have $(\lambda_x)_{max}$ up to 20δ but spanwise width restricted to $\lambda_y \sim \delta$. The overlap suggests that Φ^{w}_{cross}, like Φ, also consists of energy contributions from the superstructures which, although wall-attached, cannot be categorized as self-similar structures. The presence of these δ-scaled non-self-similar wall-attached structures has been noted previously by Baars *et al.* (2017) as well as very recently by Yoon *et al.* (2020), who also described these structures to be tall and reminiscent of the superstructures. The Φ^{w}_{cross} contour for $z_o^+ \approx 0.15\delta^+$ (figure 4a), which is centred at $\lambda_x \sim 7\delta$ and $\lambda_y \sim \delta$, can be considered representative of the energy contributions from these tall non-self-similar structures. The present analysis thus suggests that this contribution would have to be 'filtered' out from the wall-attached energy (at lower z_o^+) to obtain the 2-D spectral distribution purely from the self-similar eddies. Our conclusion aligns with the recent work of Baars & Marusic (2020), who in addition to a wall filter, also proposed a log-filter in order to isolate the energy contributions from the wall-attached self-similar eddies to the 1-D streamwise spectra. Construction of a robust log-filter, however, is challenging since it requires measurements to be conducted in a physically thick boundary layer and/or at even higher Re_τ than reported in the present study (Baars & Marusic 2020).

4. Concluding remarks

The present study investigates the 2-D cross-spectrum of u in a ZPG TBL for Re_τ spanning $O(10^3)$–$O(10^4)$. Special emphasis is laid on the cross-spectrum (Φ^{w}_{cross})

representing coherence between a log (z_o) and a near-wall reference, which depicts the energy distribution across a range of wall-attached eddies existing at z_o, and hence is a subset of the full 2-D spectrum $\Phi(z_o)$. Removal of the energy contributions from wall-detached eddies results in Φ^w_{cross}, at high Re_τ, having negligible energy contribution in the scale range where otherwise a $\lambda_y/z_o \sim (\lambda_x/z_o)^{1/2}$ behaviour is noted for Φ. Further, the energetic large scales contributing to Φ^w_{cross} follow a $\lambda_y/z_o \sim \lambda_x/z_o$ power law more closely than seen for Φ. This supports the hypothesis on the obscured view of the self-similar trend for Φ, at finite Re_τ, being a result of limited scale separation between various eddies following dissimilar scalings. Further, Φ^w_{cross} closely resembles the qualitative 2-D spectrum obtained from an AEH-based model (Φ_{AEH}), in terms of a scale-specific energy distribution as well as obeyance of the self-similar scaling laws, giving strong evidence of self-similarity ingrained in the TBL. It is shown, however, that Φ^w_{cross} does not represent energy contributions purely from self-similar eddies. At least one more filter is required to remove the contributions from wall-attached non-self-similar structures.

Acknowledgements

The authors wish to acknowledge the Australian Research Council for financial support and thank the authors of Sillero *et al.* (2014) for making their DNS data available. The authors are also grateful to the anonymous reviewers for their helpful comments which improved the quality of the manuscript.

Declaration of interests

The authors report no conflict of interest.

References

AGOSTINI, L. & LESCHZINER, M. 2017 Spectral analysis of near-wall turbulence in channel flow at $Re_\tau = 4200$ with emphasis on the attached-eddy hypothesis. *Phys. Rev. Fluids* **2** (1), 014603.

DEL ALAMO, J. C., JIMÉNEZ, J., ZANDONADE, P. & MOSER, R. D. 2004 Scaling of the energy spectra of turbulent channels. *J. Fluid Mech.* **500**, 135–144.

BAARS, W. J., HUTCHINS, N. & MARUSIC, I. 2017 Self-similarity of wall-attached turbulence in boundary layers. *J. Fluid Mech.* **823**, R2.

BAARS, W. J. & MARUSIC, I. 2020 Data-driven decomposition of the streamwise turbulence kinetic energy in boundary layers. Part 1. Energy spectra. *J. Fluid Mech.* **882**, A25.

BAIDYA, R., PHILIP, J., HUTCHINS, N., MONTY, J. P. & MARUSIC, I. 2017 Distance-from-the-wall scaling of turbulent motions in wall-bounded flows. *Phys. Fluids* **29** (2), 020712.

CHANDRAN, D. 2019 Characteristics of energetic motions in turbulent boundary layers. PhD thesis, University of Melbourne, Department of Mechanical Engineering.

CHANDRAN, D., BAIDYA, R., MONTY, J. P. & MARUSIC, I. 2016 Measurement of two-dimensional energy spectra in a turbulent boundary layer. In *Proceedings of 20th Australasian Fluid Mechanics Conference*.

CHANDRAN, D., BAIDYA, R., MONTY, J. P. & MARUSIC, I. 2017 Two-dimensional energy spectra in high-Reynolds-number turbulent boundary layers. *J. Fluid Mech.* **826**, R1.

CHAUHAN, K. A., MONKEWITZ, P. A. & NAGIB, H. M. 2009 Criteria for assessing experiments in zero pressure gradient boundary layers. *Fluid Dyn. Res.* **41** (2), 021404.

DAVIDSON, P. A., NICKELS, T. B. & KROGSTAD, P.-Å. 2006 The logarithmic structure function law in wall-layer turbulence. *J. Fluid Mech.* **550**, 51–60.

DESHPANDE, R., MONTY, J. P. & MARUSIC, I. 2019 Streamwise inclination angle of large wall-attached structures in turbulent boundary layers. *J. Fluid Mech.* **877**, R4.

HUTCHINS, N. & MARUSIC, I. 2007 Evidence of very long meandering features in the logarithmic region of turbulent boundary layers. *J. Fluid Mech.* **579**, 1–28.

HWANG, J. & SUNG, H. J. 2018 Wall-attached structures of velocity fluctuations in a turbulent boundary layer. *J. Fluid Mech.* **856**, 958–983.

KLEWICKI, J., FIFE, P. & WEI, T. 2009 On the logarithmic mean profile. *J. Fluid Mech.* **638**, 73–93.

LOZANO-DURÁN, A., FLORES, O. & JIMÉNEZ, J. 2012 The three-dimensional structure of momentum transfer in turbulent channels. *J. Fluid Mech.* **694**, 100–130.

MARUSIC, I. & MONTY, J. P. 2019 Attached eddy model of wall turbulence. *Annu. Rev. Fluid Mech.* **51**, 49–74.

MARUSIC, I., MONTY, J. P., HULTMARK, M. & SMITS, A. J. 2013 On the logarithmic region in wall turbulence. *J. Fluid Mech.* **716**, R3.

PERRY, A. E., HENBEST, S. & CHONG, M. S. 1986 A theoretical and experimental study of wall turbulence. *J. Fluid Mech.* **165**, 163–199.

PERRY, A. E. & MARUSIC, I. 1995 A wall-wake model for the turbulence structure of boundary layers. Part 1. Extension of the attached eddy hypothesis. *J. Fluid Mech.* **298**, 361–388.

ROBINSON, S. K. 1991 Coherent motions in the turbulent boundary layer. *Annu. Rev. Fluid Mech.* **23** (1), 601–639.

SILLERO, J. A., JIMÉNEZ, J. & MOSER, R. D. 2014 Two-point statistics for turbulent boundary layers and channels at Reynolds numbers up to $\delta^+ \approx 2000$. *Phys. Fluids* **26** (10), 105109.

TENNEKES, H. & LUMLEY, J. L. 1972 *A First Course in Turbulence*. MIT Press.

TOWNSEND, A. A. 1976 *The Structure of Turbulent Shear Flow*, 2nd edn. Cambridge University Press.

YOON, M., HWANG, J., YANG, J. & SUNG, H. J. 2020 Wall-attached structures of streamwise velocity fluctuations in an adverse-pressure-gradient turbulent boundary layer. *J. Fluid Mech.* **885**, A12.